

# Giant Formation Rates of Ultracold Molecules via Feshbach-Optimized Photoassociation

Philippe Pellegrini, Marko Gacesa, and Robin Côté

Department of Physics, U-3046, University of Connecticut, Storrs, Connecticut 06269-3046, USA

(Received 15 January 2008; published 1 August 2008)

Ultracold molecules offer a broad variety of applications, ranging from metrology to quantum computing. However, forming “real” ultracold molecules, i.e., in deeply bound levels, is a very difficult proposition. Here, we show how photoassociation in the vicinity of a Feshbach resonance enhances molecular formation rates by several orders of magnitude. We illustrate this effect in heteronuclear systems, and find giant rate coefficients even in deeply bound levels. We also give a simple analytical expression for the photoassociation rate and discuss future applications of the Feshbach-optimized photoassociation technique.

DOI: 10.1103/PhysRevLett.101.053201

PACS numbers: 34.50.Rk, 67.60.Fp, 67.85.-d

In recent years, several techniques, ranging from Stark decelerators to buffer-gas cooling, have been developed to obtain cold molecules [1]. Such molecules are interesting for a range of applications [2] in metrology, high precision molecular spectroscopy, or quantum computing [3]. However, forming ultracold stable molecules in deeply bound levels remains a challenge: most approaches give temperatures still considered *hot* (roughly 100 mK–1 K). To reach the ultracold regime (below 1 mK), direct laser cooling of molecules is usually not effective due to their rich and complex level structure [4]. Instead, it is possible to create molecules starting from ultracold atoms, via photoassociation (PA) or “magnetoassociation” (MA). While PA occurs when two colliding atoms absorb a photon to form a molecule [2], MA takes advantage of magnetically tuned Feshbach resonances [5].

Over the past decade, PA has been widely used to study long-range molecular interactions and to probe ultracold gases [2], and MA to realize molecular condensates [6] and investigate the Bose-Einstein condensation (BEC)-BCS crossover regime [7]. However, both methods usually lead to molecules in highly excited states. According to the Franck-Condon principle, electronic transitions in PA occur at large interatomic distances, leading to molecules in high rovibrational levels that can either decay by spontaneous emission or collisional quenching. To stabilize the molecules in their ground potentials, one could use two-photon schemes [8] or excited molecular states with long-range wells that increase the probability density at short range. This latter solution requires the existence of double-well molecular potentials [4] and cannot be easily generalized. In MA, molecules are produced by sweeping the magnetic field through a Feshbach resonance, which occurs when the energy of a colliding pair of atoms matches that of a bound level associated to a closed channel. The molecules produced by MA are in the uppermost states near dissociation [5] and thus relatively extended and fragile.

In this Letter, we investigate a new PA scheme which uses a magnetically induced Feshbach resonance [5] to enhance the probability density at short range. This

Feshbach-optimized photoassociation (FOPA) allows transitions even to deeply bound levels (see Fig. 1). Combining Feshbach resonances and PA has been proposed to associate atoms [9] and convert an atomic into a molecular BEC [10]. However, as opposed to previous proposals based on the Franck-Condon principle [11], FOPA takes advantage of the whole wave function in a full quantum coupled-channel calculation, and is thus more general.

Feshbach resonances commonly occur in systems with hyperfine interactions. We focus our attention on heteronuclear systems for which the presence of a permanent dipole moment allows transitions from the continuum directly to a rovibrational level  $\nu$  of the ground electronic molecular states [12] (see Fig. 1). The corresponding photoassociation rate coefficient  $K_{\text{PA}}^{\nu} = \langle v_{\text{rel}} \sigma_{\text{PA}}^{\nu} \rangle$  [2,8] depends on  $v_{\text{rel}}$ , the relative velocity of the colliding pair, and on  $\sigma_{\text{PA}}^{\nu}$ , the PA cross section. The brackets stand for an

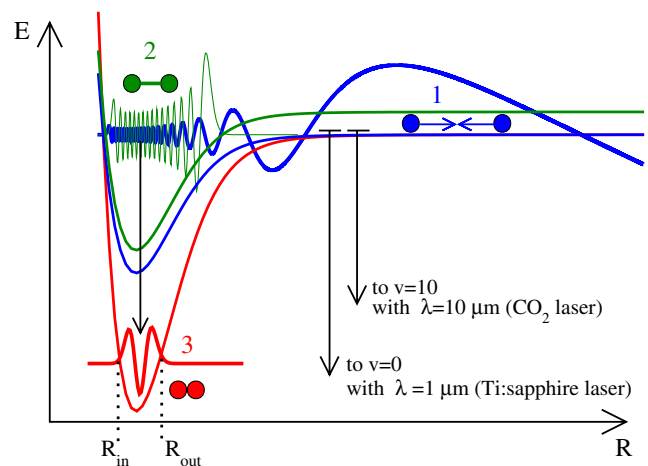


FIG. 1 (color online). FOPA: Colliding atoms (1) interact via open (blue) and closed (green) channels due to hyperfine interactions. A Feshbach resonance occurs when a bound level (2) (green wave function) coincides with the continuum state (blue wave function). A photon (wavelength  $\lambda$ ) can associate the atoms into a bound level  $\nu$  (3) of the ground state potential (red) with inner and outer classical turning points  $R_{\text{in}}$  and  $R_{\text{out}}$ .

average over the distribution of  $v_{\text{rel}}$ , here a Maxwell-Boltzmann distribution characterized by the temperature  $T$  [13]. At low laser intensity  $I$  and ultracold temperatures, where only the  $s$  wave contributes significantly, the maximum rate coefficient (neglecting saturation) is [12]

$$K_{\text{PA}}^v = \frac{8\pi^3}{h^2} \frac{I}{c} \frac{e^{-1/2}}{Q_T} |\langle \phi_{v,J=1} | D(R) | \Psi_{\epsilon,l=0} \rangle|^2, \quad (1)$$

where  $Q_T = (2\pi\mu k_B T/h^2)^{3/2}$ , and  $D(R)$  is the appropriate dipole moment for the transition between the initial  $|\Psi_{\epsilon,l=0}\rangle$  and final  $|\phi_{v,J=1}\rangle$  states corresponding to the  $s$  wave ( $l=0$ ) continuum wave function of the colliding pair and the populated bound level ( $v, J=1$ ) wave function. Here  $k_B$ ,  $h$ , and  $c$  are the Boltzmann and Planck constants and the speed of light in vacuum, respectively.

We determine  $|\Psi_{\epsilon,l=0}\rangle$  by solving the Hamiltonian for two colliding atoms in a magnetic field [5]:

$$H = \frac{p^2}{2\mu} + V_C + \sum_{j=1}^2 H_j^{\text{int}}. \quad (2)$$

Here,  $V_C = V_0(R)P^0 + V_1(R)P^1$  is the Coulomb interaction, decomposed into singlet ( $V_0$ ) and triplet ( $V_1$ ) molecular potentials, with the associated projection operator  $P^0$  and  $P^1$ . The internal energy of atom  $j$ ,  $H_j^{\text{int}} = \frac{a_{\text{hf}}^{(j)}}{h^2} \vec{s}_j \cdot \vec{i}_j + (\gamma_e \vec{s}_j - \gamma_n \vec{i}_j) \cdot \vec{B}$ , consists of the hyperfine and Zeeman contributions, respectively. Here  $\vec{s}_j$  and  $\vec{i}_j$  are the electronic and nuclear spin of atom  $j$  with hyperfine constant  $a_{\text{hf}}^{(j)}$ , and  $\vec{B}$  is the magnetic field. Since the nuclear gyromagnetic factor  $\gamma_n$  is 3 orders of magnitude smaller than  $\gamma_e$ , we neglect it in our calculations.

We solve for  $|\Psi_{\epsilon,l=0}\rangle$  by using the mapped Fourier grid method [14], and by expanding it onto the basis constructed from the hyperfine states of both atoms,

$$|\Psi_{\epsilon,l=0}\rangle = \sum_{\sigma=1}^N \psi_{\sigma}(R) \{|f_1, m_1\rangle \otimes |f_2, m_2\rangle\}_{\sigma}, \quad (3)$$

where  $\vec{f}_j = \vec{i}_j + \vec{s}_j$  is the total spin of atom  $j$ , and  $m_j$  its projection on the magnetic axis. Here,  $\psi_{\sigma}(R)$  stands for the radial wave function associated with channel  $\sigma$  labeled by the quantum numbers  $f_j, m_j$ . As an example, we consider forming LiNa in the  $X^1\Sigma^+$  state starting with  ${}^6\text{Li}(f = \frac{1}{2}, m = -\frac{1}{2})$  and  ${}^{23}\text{Na}(f = 1, m = -1)$ . Eight channels with total projection  $M = m_1 + m_2 = -\frac{3}{2}$  are coupled by the Hamiltonian (2), and using the potentials in [15], we find two well-separated Feshbach resonances at 1081 G (narrow) and 1403 G (broad). These are better suited to extract the underlying physics than three observed overlapping narrow resonances [15,16], and a broad resonance should help optimize the process while minimizing three-body losses. Figure 2 displays  $K_{\text{PA}}^v$  as a function of the  $B$  field into different levels ( $v, J=1$ ) at  $T = 50 \mu\text{K}$  and  $I = 1 \text{ W/cm}^2$ . Near a resonance,  $K_{\text{PA}}^v$  is drastically enhanced by up to 5 orders of magnitude, even for the lowest ( $v <$

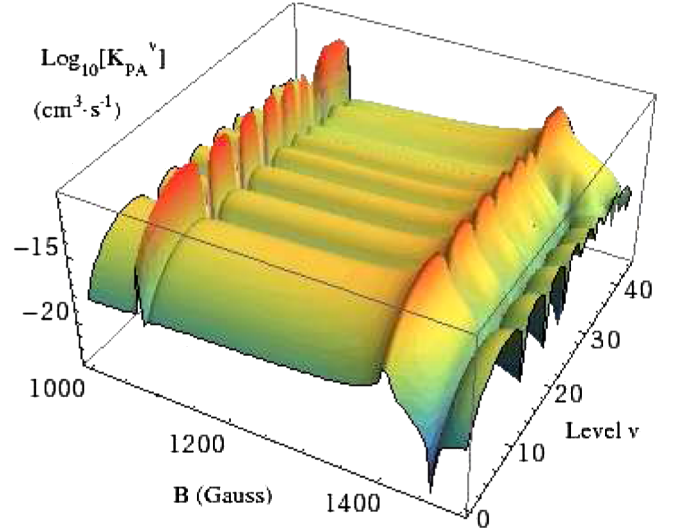


FIG. 2 (color online).  $K_{\text{PA}}^v$  in  $\text{cm}^3/\text{s}$  versus the  $B$  field ( $T = 50 \mu\text{K}$ ,  $I = 1 \text{ W/cm}^2$ ) for various levels ( $v, J=1$ ) of the LiNa  $X^1\Sigma^+$  potential, starting from  ${}^6\text{Li}(f = \frac{1}{2}, m = -\frac{1}{2})$  and  ${}^{23}\text{Na}(f = 1, m = -1)$ . Two Feshbach resonances at 1081 and 1403 G enhance the PA rates by several orders of magnitude.

10) levels. For example, with typical densities ( $n_{\text{Li}} = n_{\text{Na}} \sim 10^{12} \text{ cm}^{-3}$ ) and an illuminated volume  $V$  of  $1 \text{ mm}^3$ ,  $N_v = n_{\text{Li}} n_{\text{Na}} V K_{\text{PA}}^v = 2 \times 10^6$  molecules/sec are formed in  $v = 0$  at 1403 G (neglecting back stimulation [8]).

These giant formation rates can be understood by the sharp increase in the amplitudes of the  $\psi_{\sigma}$ 's in the vicinity of a Feshbach resonance. In Fig. 3, we show the total probability density  $|\Psi_{\epsilon,l=0}(R)|^2$  as a function of  $B$ . As the magnetic field  $B$  nears either of the resonances at 1081 and 1403 G,  $|\Psi_{\epsilon,l=0}(R)|^2$  increases by several orders of magnitude (qualitatively the same for all channels). Figure 4 shows  $|\Psi_{\epsilon,l=0}(R)|^2$  for two specific values of  $B$

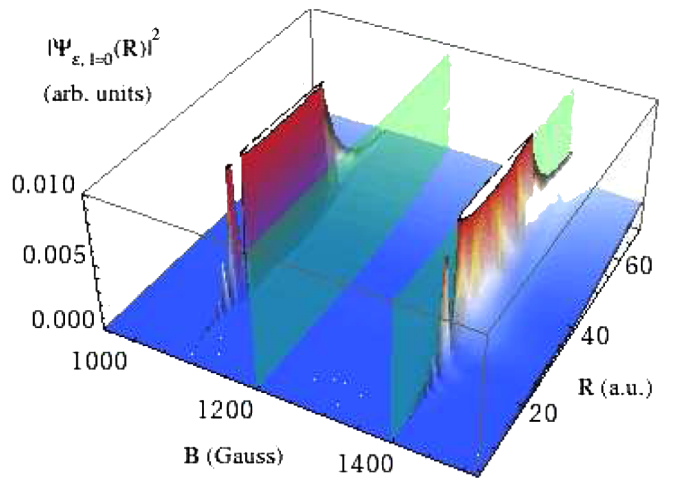


FIG. 3 (color online). Probability density  $|\Psi_{\epsilon,l=0}(R)|^2$  vs  $B$ . As  $B$  nears a resonance,  $|\Psi_{\epsilon,l=0}|^2$  increases sharply (truncated above 0.01). Examples of  $|\Psi_{\epsilon,l=0}|^2$  off and on resonance (green planes at 1200 and 1400 G, respectively) are shown in Fig. 4.

on and off resonance (1400 and 1200 G, respectively): the resonance leads to a large peak at shorter  $R$  near  $40 a_0$  (see top panel, inset). This peak is roughly located at the classical outer turning point  $R_{\text{out}}$  of the bound state associated to the closed channel, usually one of the uppermost bound levels. This is apparent in the top panel, where this peak almost coincides with the outer lobe of  $|\phi_{v=44, l=1}(R)|^2$ , the uppermost bound level of  $X^1\Sigma^+$ . We also observe that the off-resonance probability density is very much reduced when compared to on-resonance, leading to a very weak overlap integral in  $K_{\text{PA}}^v$ . The lower panel zooms on the short range, where  $|\Psi_{\epsilon, l=0}(R)|^2$  on resonance is much larger than off resonance, leading to a substantial overlap integral in  $K_{\text{PA}}^v$  with deeply bound levels (e.g.,  $v = 0$  or 4). We also note that the more complicated nodal structure of  $|\Psi_{\epsilon, l=0}(R)|^2$  is a direct result of the hyperfine mixing among channels.

Analytical results are obtained with a two coupled channel model of reduced mass  $\mu$ , in which the wave function  $\psi_1$  of the continuum state associated to the open channel 1 (with potential  $V_1$ ) is coupled to the wave function  $\psi_2$  associated to the closed channel 2 (with  $V_2$ ) [17]

$$-\frac{\hbar^2}{2\mu} \frac{d^2}{dR^2} \begin{pmatrix} \psi_1 \\ \psi_2 \end{pmatrix} + \begin{pmatrix} V_1 & V_{1,2} \\ V_{2,1} & V_2 \end{pmatrix} \begin{pmatrix} \psi_1 \\ \psi_2 \end{pmatrix} = E \begin{pmatrix} \psi_1 \\ \psi_2 \end{pmatrix}. \quad (4)$$

We assume both couplings  $V_{1,2}$  and  $V_{2,1}$  real, and fix the threshold  $E_1$  of channel 1 at  $E = 0$ . If the couplings were switched off, the solution for channel 1 would be  $\psi_1 \rightarrow$

$\psi_{\text{reg}}$  (regular solution defined below) while the closed channel 2 would have a bound state  $\psi_2 \rightarrow \psi_0$  with energy  $E_0$ . A resonance occurs when  $E$  nears  $E_0$ . The analytical solutions for Eq. (4) are then [17]

$$\psi_1(R) = \psi_{\text{reg}}(R) + \tan\delta\psi_{\text{irr}}(R)$$

$$\stackrel{R \rightarrow \infty}{=} \frac{1}{\cos\delta} \sqrt{\frac{2\mu}{\pi\hbar^2 k}} \sin(kR + \delta_{\text{bg}} + \delta), \quad (5)$$

$$\psi_2(R) = -\sqrt{\frac{2}{\pi\Gamma}} \sin\delta\psi_0(R), \quad (6)$$

where  $\delta_{\text{bg}}$  and  $\delta$  are the background and resonant phase shifts, while  $k = \sqrt{2\mu E}/\hbar$ . The asymptotic regular and irregular solutions are  $\psi_{\text{reg}} = \sqrt{\frac{2\mu}{\pi\hbar^2 k}} \sin(kR + \delta_{\text{bg}})$  and  $\psi_{\text{irr}} = \sqrt{\frac{2\mu}{\pi\hbar^2 k}} \cos(kR + \delta_{\text{bg}})$ . Finally, the width  $\Gamma(E)$  of the resonance may vary slowly with  $E$ .

Here, scanning the  $B$  field is equivalent to scanning  $E$ , since the position  $E_0$  of the bound state in channel 2 is shifted by the Zeeman interaction. To first order in  $k$ , the  $s$ -wave phase shifts are related to the scattering length  $a$  by  $\tan(\delta + \delta_{\text{bg}}) = -ka$ , with  $\delta_{\text{bg}} = -ka_{\text{bg}}$  and [5]

$$a = a_{\text{bg}} \left( 1 - \frac{\Delta}{B - B_0} \right), \quad (7)$$

where  $a_{\text{bg}}$  is the background scattering length of the pair of atoms (which can slowly vary with  $B$ ),  $B_0$  is the position of resonance, and  $\Delta$  is related to  $\Gamma(E)$  [5]. Introducing the analytical solutions into Eq. (1) leads to

$$K_{\text{PA}}^v = K_{\text{off}}^v |1 + C_1 \tan\delta + C_2 \sin\delta|^2, \quad (8)$$

where  $K_{\text{off}}^v = \frac{8\pi^3}{h^2} \frac{I}{c} \frac{e^{-1/2}}{Q_T} |\langle \psi_v | D | \psi_{\text{reg}} \rangle|^2$  is the rate coefficient off resonance ( $\delta = 0$ ) with  $\psi_v$  the final (target) state, and  $C_1 = \langle \psi_v | D | \psi_{\text{irr}} \rangle / \langle \psi_v | D | \psi_{\text{reg}} \rangle$  and  $C_2 = -\sqrt{2/\pi\Gamma} \langle \psi_v | D | \psi_0 \rangle / \langle \psi_v | D | \psi_{\text{reg}} \rangle$  relate to the open channel 1 and the closed channel 2, respectively.

The relative importance of  $C_1$  and  $C_2$  depends on the nodal structure of  $\psi_v$ ,  $\psi_{\text{reg}}$ ,  $\psi_{\text{irr}}$ , and  $\psi_0$ . Unless  $R_{\text{out}}$  of  $\psi_v$  accidentally coincides with a node in  $\psi_{\text{reg}}$  or  $\psi_{\text{irr}}$ , the overlap integral of  $\psi_v$  with both  $\psi_{\text{reg}}$  and  $\psi_{\text{irr}}$  are of the same order, leading to  $|C_1| \sim 1$ . The relative size of  $C_2$  can be controlled by the target level  $v$ . For a deeply bound level,  $R_{\text{out}}$  is at short separation where the overlap with  $\psi_{\text{reg}}$  is small while the overlap with  $\psi_0$  can be substantial leading to  $|C_2| \gg |C_1|$ . For very extended levels  $v$ ,  $R_{\text{out}}$  of  $\psi_v$  is at large separation and the overlap with  $\psi_0$  less important, leading to  $|C_2| \ll |C_1|$ . Naturally, these behaviors might differ for specific levels  $v$ .

The generalization of Eq. (8) to several coupled channels is straightforward. Furthermore, we find that only two or three channels contribute significantly to give these giant formation rate coefficients. In Fig. 5, we show  $K_{\text{PA}}^v$  for  $v = 0$  with the same parameters used in Fig. 2. The top panel depicts the scattering length  $a$  with the two Feshbach resonances and its analytical fit. The bottom panel com-

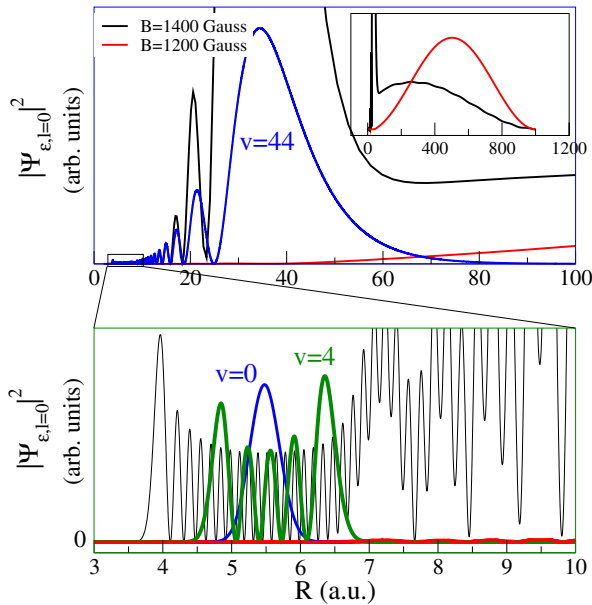


FIG. 4 (color online).  $|\Psi_{\epsilon, l=0}(R)|^2$  on (black) and off (red) resonance. The top panel shows a peak appearing near  $R \sim 40$  a.u. on resonance (inset). The upper bound level  $v = 44$  of  $X^1\Sigma^+$  is also depicted. The off-resonance density is negligible for  $R < 50$  a.u. The bottom panel illustrates the inner region with more deeply bound target levels (e.g.,  $v = 0$  and 4). Again,  $|\Psi_{\epsilon, l=0}|^2$  is sizable on resonance and negligible off resonance.

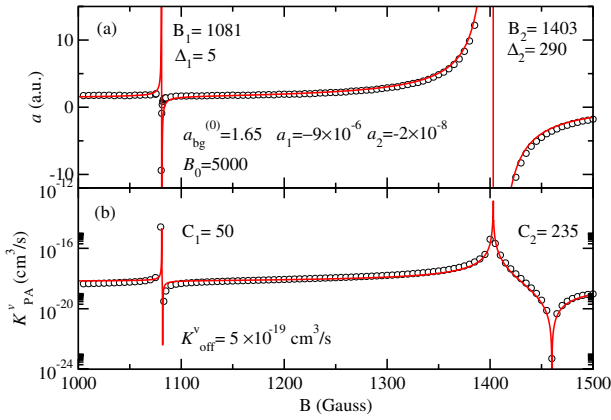


FIG. 5 (color online). In (a) scattering length  $a$  for full coupled problem (circles) and the fit using  $a = a_{bg}(B)(1 - \frac{\Delta_1}{B-B_1} - \frac{\Delta_2}{B-B_2})$  with  $a_{bg}(B) = a_{bg}^{(0)} + a_1(B + B_0) + a_2(B + B_0)^2$ . In (b)  $K^v_{PA}$  for  $v = 0$  at  $50 \mu\text{K}$  and  $1 \text{ W}/\text{cm}^2$  (circles) and the formula (8) using  $\tan \delta = ka_{bg}(B)(\frac{\Delta_1}{B-B_1} + \frac{\Delta_2}{B-B_2})$ , with  $C_1$  and  $C_2$   $B$ -independent. Numerical parameters are given in each plot.

compares the exact numerical results using eight coupled channels with the simple expression (8). In both cases, the agreement is impressive. We verified that similar agreement was obtainable for other levels  $v$ , indicating the broad and general validity of Eq. (8).

In conclusion, we showed that it is possible to use Feshbach-optimized photoassociation to form “real” ultracold molecules, i.e., in deeply bound levels, in large quantities. In fact, the rate coefficient increases by several orders of magnitude, leading to giant formation rates near Feshbach resonances. We applied this concept to LiNa, a polar molecule, and found rates of  $\sim 10^6$  molecules/sec into low  $v$ 's, assuming a 50% efficiency due to back stimulation and inhomogeneity of the  $B$  field. This compares well with recent results based on a combination of MA and stimulated Raman adiabatic passage (STIRAP) where about 80% of 20 000 Feshbach molecules are transferred into deeper levels in a cycle (cooling + forming Feshbach molecules) of tens of seconds [18]. In addition, we gave a simple analytical model describing the FOPA technique. As opposed to other proposals based on the Franck-Condon principle for transition near the turning point  $R_{out}$  of the closed channel, FOPA takes advantage of the full wave function and its amplification in the vicinity of a Feshbach resonance, making it a general technique. In fact, FOPA could be used to do the spectroscopy of more deeply bound levels of excited electronic states which are usually not reachable by standard PA, bridging the gap between traditional spectroscopy for deep levels and PA of high-lying levels realized with ultracold atoms. Also, by targeting levels  $v$  for which  $C_1$  or  $C_2$  is dominant, it is possible to determine the parameters of the scattering length ( $a_{bg}$ ,  $\Delta$ , and  $B_0$ ) by pure spectroscopic measurements. This offers an accurate nondestructive method to first detect a Feshbach resonance, and then

obtain the scattering length parameters. Finally, we note that this enhancement will be present in other manifestations of Feshbach resonances, such as those obtained via electric fields [19] or magnetic dipolar interactions (e.g., in Cr [20]). This is a very general technique which can be applied to bosonic, fermionic, or mixed species, where Feshbach resonances exist.

This research was supported by the U.S. Department of Energy, Office of Basic Energy Sciences.

- [1] J. Doyle *et al.*, Eur. Phys. J. D **31**, 149 (2004), and references therein.
- [2] K.M. Jones, E. Tiesinga, P.D. Lett, and P.S. Julienne, Rev. Mod. Phys. **78**, 483 (2006).
- [3] D. DeMille, Phys. Rev. Lett. **88**, 067901 (2002); S.F. Yelin, K. Kirby, and R. Côté, Phys. Rev. A **74**, 050301(R) (2006).
- [4] A. Fioretti *et al.*, Phys. Rev. Lett. **80**, 4402 (1998); M.D. Di Rosa, Eur. Phys. J. D **31**, 395 (2004).
- [5] T. Köhler, K. Góral, and P.S. Julienne, Rev. Mod. Phys. **78**, 1311 (2006).
- [6] S. Jochim *et al.*, Science **302**, 2101 (2003); M. Greiner, C.A. Regal, and D.S. Jin, Nature (London) **426**, 537 (2003); M.W. Zwierlein *et al.*, Phys. Rev. Lett. **91**, 250401 (2003).
- [7] D.E. Miller *et al.*, Phys. Rev. Lett. **99**, 070402 (2007); A. Altmeyer *et al.*, Phys. Rev. Lett. **98**, 040401 (2007); G.B. Partridge *et al.*, Phys. Rev. Lett. **95**, 020404 (2005); M. Greiner, C.A. Regal, and D.S. Jin, Phys. Rev. Lett. **94**, 070403 (2005).
- [8] E. Juarros, R. Côté, and K. Kirby, Eur. Phys. J. D **31**, 213 (2004); E. Juarros, K. Kirby, and R. Côté, J. Phys. B **39**, S965 (2006).
- [9] F.A. van Abeelen *et al.*, Phys. Rev. Lett. **83**, 1550 (1999).
- [10] S.J.J.M.F. Kokkelmans, H.M.J. Vissers, and B.J. Verhaar, Phys. Rev. A **63**, 031601 (2001); T. Hornung, S. Gordienko, R. de Vivie-Riedle, and B.J. Verhaar, Phys. Rev. A **66**, 043607 (2002).
- [11] B. Laburthe *et al.*, Europhys. Lett. **64**, 171 (2003); W.C. Stwalley, Eur. Phys. J. D **31**, 221 (2004); F.A. van Abeelen, D.J. Heinzen, and B.J. Verhaar, Phys. Rev. A **57**, R4102 (1998).
- [12] E. Juarros, P. Pellegrini, K. Kirby, and R. Côté, Phys. Rev. A **73**, 041403(R) (2006).
- [13] This  $T$  dependence is valid at all  $T$  for mixed species.
- [14] V. Kokkoulina, O. Dulieu, R. Kosloff, and F. Masnou-Seeuws, J. Chem. Phys. **110**, 9865 (1999).
- [15] M. Gacesa, P. Pellegrini, and R. Côté, arXiv:0709.2924.
- [16] C.A. Stan *et al.*, Phys. Rev. Lett. **93**, 143001 (2004).
- [17] Harald Friedrich, *Theoretical Atomic Physics* (Springer-Verlag, Berlin, 1990).
- [18] K. Winkler *et al.*, Phys. Rev. Lett. **98**, 043201 (2007); S. Ospelkaus *et al.*, Nature Phys., doi:10.1038/nphys997 (2008).
- [19] Z. Li and R. V. Krems, Phys. Rev. A **75**, 032709 (2007).
- [20] J. Werner *et al.*, Phys. Rev. Lett. **94**, 183201 (2005); Z. Pavlovic, R. V. Krems, R. Côté, and H.R. Sadeghpour, Phys. Rev. A **71**, 061402(R) (2005).